Electric Power Systems Research, 25 (1992) 227–238

A fuzzy logic power tracking controller for a photovoltaic energy conversion scheme

I. H. Altas and A. M. Sharaf*

Electrical Engineering Department, University of New Brunswick, P.O. Box 4400, Fredericton, N.B., E3B 5A3 (Canada)

(Received June 25, 1992)

Abstract

The maximum solar power tracking and energy utilization of a stand-alone photovoltaic array (PVA) feeding a chopper controlled permanent magnet DC motor drive scheme is studied. A computer controlled model of the PVA including the effects of temperature and solar irradiation changes was developed and used in both digital simulation and laboratory implementation. The electrical load applied voltage was controlled by a MOSFET type-A chopper using either proportional–integral or fuzzy logic based controllers so that the maximum available solar power of the PVA is always tracked for all varying ambient temperature and solar irradiation levels, as well as for any small variations of the electrical load. The dynamic performance of the overall system was studied and satisfactory results were obtained using both types of controller.

1. Introduction

The use of new efficient photovoltaic solar cells (PVSCs) has emerged as an important solution in energy conservation and demand-side management during the last decade. Owing to their initial high costs, PVSCs have not yet been an attractive alternative for electricity users who are able to buy cheaper electrical energy from the utility grid. However, they have been used extensively for water pumping and air conditioning in remote and isolated areas where utility power is not available or is too expensive to transport. Although solar cell (SC) prices have decreased considerably during the last years due to new developments in the film technology and manufacturing process [1], PV arrays are still considered rather expensive compared with the utility fossil fuel generated electricity prices. After building such an expensive renewable energy system, the user naturally wants to operate the PV array at its highest conversion efficiency by continuously utilizing the maximum available output power of the array. The electrical system powered by solar cells requires special design considerations because of the varying nature of the solar power generated resulting from unpredictable changes in weather conditions which affect the solar radiation level as well as the cell operating temperature. Salameh and Dagher [2] have proposed a switching system that changes the cell array topology and connections or the configurations of the cells to get the required voltage during different periods of a day. A steady-state analysis of a scheme employing direct coupling between a series/shunt or separately excited DC motors and the photovoltaic solar arrays has been given by Roger [3]. The dynamic performance of a DC shunt motor–photovoltaic system has been studied by Fam and Balachander [4]. The starting and steady-state characteristics of DC motors powered by a solar cell array source have been studied by Appelbaum [5] to select the suitable parameters and type of DC motor for a desired utilization scheme. All these studies concerning DC motors or permanent magnet (PM) DC motors powered by PV generators have been done by considering the direct interface between the motor load and the PV source generator. For direct coupling of DC motors to solar arrays, the separately excited or PM motors with a ventilator type load are the most suitable [5]. Owing to changes in the solar radiation energy and the cell operating temperature, the output power of a solar array is not constant at all times. Consequently, a maximum solar power tracking controller is always needed in any scheme with solar cell arrays [6, 7] to

*Currently Visiting Professor at Nanyang Technological University, Singapore.

0378-7796/92/$5.00

ensure maximum utilization. Maximum solar power tracking strategies have mostly been studied for direct interface with the electrical load or with a large AC utility grid using controllable solid-state power converters between the PV source and utility grid.

The output power of a PV array when directly coupled to the electrical load is defined by the electrical load power setting on the volt–ampere curve. If the load power, voltage and current are not exactly the same as those corresponding to the available maximum power levels of the array at any given insolation level, then the PV array operates at lower output power, thus wasting some of the solar energy which is already available for conversion. Using a controllable interface converter stage instead of direct coupling, the PV array can be operated always at its maximum power reference point, irrespective of variations in ambient temperature, solar irradiation, as well as small excursions in the electrical load. As shown in Fig. 1, the proposed PV array–DC load scheme uses a MOSFET converter chopper as a variable equivalent matching device between the PV array and the electrical load. The chopper operates the PV array at the maximum power reference point under the effects of variations in ambient temperature, solar irradiation, and load excursions.

The PC based emulation model of the PV array characteristics is stored in an IBM AT computer and interfaced with the electrical load system using a Data Translation DT2821 data acquisition board and the ATLAB software drivers. The temperature input is entered in terms of the variable analog reference voltage, and the solar irradiation level is obtained based on this temperature input. The array voltage is calculated as a function of this temperature reference, solar irradiation, and load current. The array voltage reference is then amplified to a value equal to or higher than the value of the applied load voltage. This voltage is 'chopped' by the chopper converter interface and applied to the DC motor so that the resultant equivalent motor current forces the PV array to operate at the voltage level that coincides with the voltage value at the maximum power reference point. The chopping period or the duty cycle ratio α_D of the MOSFET chopper is determined by the controller driven by the mismatch error $\theta_e = (\theta_M - \theta_C)$ of the PV array. The error is an offset angle between the ideal maximum power line and the operating electric power line in the per unit current–voltage (I–V) characteristics of the PV array as shown later in Fig. 4. The controller used in the scheme can be either a classical proportional–integral (PI) controller or a fuzzy logic (FL) based controller. For many years, the classical PI controllers have been used widely in different applications, including those of the photovoltaic energy systems interfaced with the utility grid. The use of the proposed fuzzy logic controllers, however, started in the mid 1970s after Mamdani and his colleagues controlled an industrial plant comprising a steam engine and boiler combination [8–10] using the fuzzy set theory rules introduced by Zadeh [11, 12]. Since the introduction of fuzzy logic controllers there has been considerable interest in the subject, with extensive research in the literature [13]. However, none of this research dealt with the on-line application of FL controllers to photovoltaic utilization systems. In the proposed scheme an on-line fuzzy logic controller was used to track the maximum available solar power output of a PV array. A PI controller was used for the same scheme to compare the performance and assess the fuzzy logic control response adequacy and robustness.

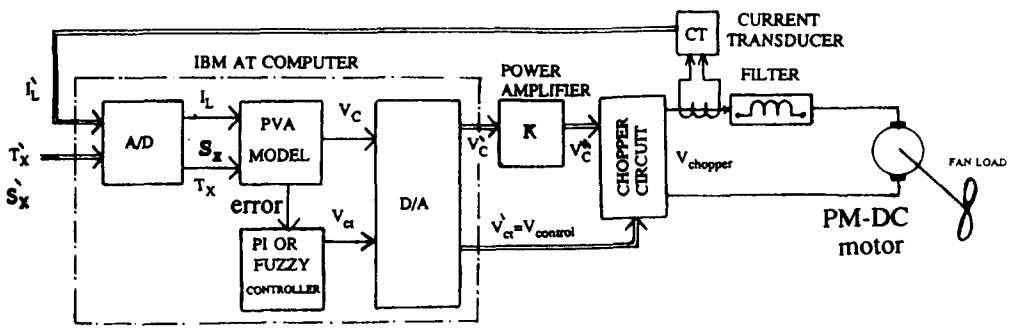

Fig. 1. Schematic diagram of the system.

2. Maximum power point operation of the PV array

PV arrays are built up with series/parallel connected combinations of solar cells. A solar cell is usually represented by the equivalent circuit given in Fig. 2(a) resulting in the current equation

$$I_C = I_{ph} - I_0\left\{\exp\left[\frac{e}{kT_C}(V_C + R_S I_C)\right] - 1\right\} - \frac{V_C + R_S I_C}{R_{sh}} \quad (1)$$

The symbols are defined as follows.

- e electron charge (1.106×10^{-19} C)
- k Boltzmann constant (0.138×10^{-23} J/K)
- I_C cell output current, A
- I_{ph} photocurrent, function of irradiation level and junction temperature (0.108 A)
- I_0 reverse saturation current of diode D (0.0002 A)
- R_S series resistance of cell (0.001 Ω)
- R_{sh} parallel resistance of cell, Ω
- T_C reference cell operating temperature (20 °C)
- V_C cell output voltage, V

Both k and T_C should have the same temperature unit, either Kelvin or Celsius. Since the shunt resistance R_{sh} is much greater than the series resistance R_S, the last term in eqn. (1) becomes very small compared with the sum of the other terms. Therefore, the last term will be neglected as it will not cause a large error in the PV emulation model; hence, eqn. (1) can now be modified to the form

$$I_C \cong I_{ph} - I_0\left\{\exp\left[\frac{e}{kT_C}(V_C + R_S I_C)\right] - 1\right\} \quad (2)$$

Equation (2) can be represented by the amplified equivalent circuit shown in Fig. 2(b).

Use of the nonlinear equation form $V_C = f(I_C)$ instead of the form $I_C = f(V_C)$ of eqns. (1) and (2) is easier for computer emulation because the cell current I_C is determined from the load current and is used to calculate the corresponding cell output voltage V_C as follows:

$$V_C = \frac{AkT_C}{e}\ln\left(\frac{I_{ph} + I_0 - I_C}{I_0}\right) - R_S I_C \quad (3)$$

The curve fitting factor A is used to adjust the I–V characteristics of the cell obtained from eqn. (3) to the actual characteristics of the cell. This equation gives the voltage of a single solar cell which is then multiplied by the number of the cells connected in series to calculate the full array voltage. Before being used again in eqn. (3), the cell current I_C is obtained by dividing the full array current, which is effectively equal to the electrical load current, by the number of the cells connected in parallel. Equation (3) is only valid for a certain cell operating temperature T_C with its corresponding solar irradiation level S_C. If the temperature and solar irradiation levels change, the voltage and current outputs of the PV array will follow this change. Hence, the effects of the changes in temperature and solar irradiation levels should also be included in the final PV array emulator. A method to include these effects in the PV array modelling is given by Buresch [1]. According to his method, for a known temperature and a known solar irradiation level, a model is obtained and then this model is modified to handle different cases of temperature and irradiation levels. Let eqn. (3) be the benchmark model for the known operating temperature T_C and known solar irradiation level S_C as given in the specification. When the ambient temperature and irradiation levels change, the cell operating temperature also changes, resulting in a new output voltage and a new photocurrent value. The solar cell operating temperature varies as a function of solar irradiation level and ambient temperature. The variable ambient temperature T_a affects the cell output voltage and cell photocurrent. These effects are represented in the model by the temperature coefficients C_{TV} [1] and C_{TI} for cell output voltage and cell photocurrent, respectively:

$$C_{TV} = 1 + \beta_T(T_a - T_X) \quad (4)$$

$$C_{TI} = 1 + \frac{\gamma_T}{S_C}(T_X - T_a) \quad (5)$$

where $\beta_T = 0.004$ and $\gamma_T = 0.06$ for the cell used and T_a is the ambient temperature during the cell testing. This is used to obtain the modified model of the cell for another ambient temperature

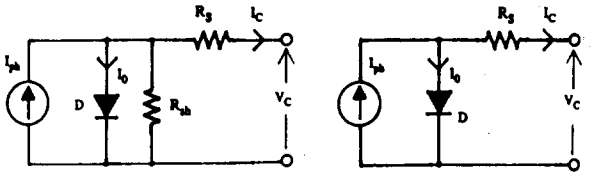

(a) (b)

Fig. 2. Equivalent circuit models of a PV cell: (a) actual cell model; (b) simplified cell equivalent circuit.

T_X. Even if the ambient temperature does not change significantly during the daytime, the solar irradiation level changes depending on the amount of sunlight and clouds. A change in solar irradiation level causes a change in the cell photocurrent and operating temperature, which in turn affects the cell output voltage. If the solar irradiation level increases from S_{C1} to S_{C2}, the cell operating temperature and the photocurrent will also increase from T_{C1} to T_{C2} and from I_{ph1} to I_{ph2}, respectively. Thus the change in the operating temperature and in the photocurrent due to variation in the solar irradiation level can be expressed via two constants, C_{SV} and C_{SI}, as correction factors for changes in cell output voltage V_C and photocurrent I_{ph}, respectively:

$$C_{SV} = 1 + \beta_T \alpha_S (S_X - S_C) \tag{6}$$

$$C_{SI} = 1 + \frac{1}{S_C}(S_X - S_C) \tag{7}$$

where S_C is the benchmark reference solar irradiation level during the cell testing to obtain the modified cell model. S_X is the new level of the solar irradiation. The temperature change ΔT_C occurs due to the change in the solar irradiation level and is obtained using

$$\Delta T_C = \alpha_S (S_X - S_C) \tag{8}$$

The constant α_S represents the slope of the change in the cell operating temperature for a change in the solar irradiation level [1] and is equal to 0.2 for the solar cells used. Using correction factors C_{TV}, C_{TI}, C_{SV} and C_{SI}, the new values of the cell output voltage V_{CX} and photocurrent I_{phX} are obtained for the new temperature T_X and solar irradiation S_X as follows:

$$V_{CX} = C_{TV} C_{SV} V_C \tag{9}$$

$$I_{phX} = C_{TI} C_{SI} I_{ph} \tag{10}$$

where C_{TV} and C_{TI} represent the effect of the ambient temperature variations as given in eqns. (4) and (5), and C_{SV} and C_{SI} represent the solar irradiation changes as given in eqns. (6) and (7). V_C and I_{ph} are the benchmark reference cell output voltage and reference cell photocurrent, respectively. The resulting $I-V$ and $P-V$ curves for changes in irradiation and temperature levels are given in Figs. 3(a) and (b), respectively.

The reverse saturation current I_0 of the diode in the equivalent circuit model is much smaller than the photocurrent I_{ph} during the short-circuit condition and can be neglected. Thus, we can assume I_{ph} to be approximately equal to the short-circuit current I_{SC}. Therefore, for each new

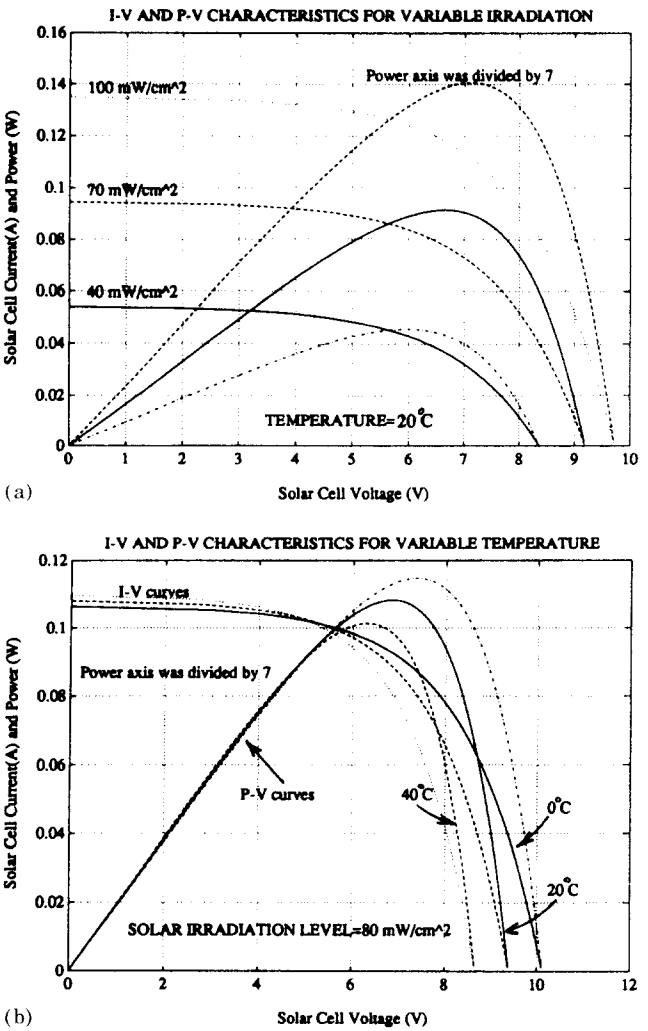

Fig. 3. $I-V$ and $P-V$ curves of the solar cell model representing (a) variable solar irradiation and (b) variable temperature.

value I_{phX} of the photocurrent, there will be a new value I_{SCX} of the short-circuit current on the $I-V$ characteristics.

After adjusting the model, the current–voltage ($I-V$) and the power–voltage ($P-V$) characteristics of the array can easily be obtained for different temperature and irradiation levels. The maximum power operating points at different temperatures and irradiation levels are determined then either stored in a look-up table or expressed by a curve fitted polynomial equation. Here, the polynomial representations of the resultant maximum power point P_{CM}, current I_{CM} at maximum power, and voltage V_{CM} at maximum power are used. The coefficients of these polynomial equations are found by least square curve fitting of the known P_{CM}, V_{CM}, and I_{CM} values. Using the resultant polynomial model, the maxi-

mum power points are calculated for any temperature and solar irradiation level at which the array is being operated and then are compared with the other operating point values. The differences between the reference maximum power point and the load operating point is called the maximum power point error. In order to track available solar power and operate the array at its maximum power point at all times, the error should be minimized at all times. Consider the normalized $I-V$ characteristics of the PV array with the three operating points given in Fig. 4.

The maximum power point (MPP) level has been chosen as the reference or preset value to simplify error tracking and keep the MPP constant on the per unit curve representation. Therefore, whatever the operating and ambient temperature, the related current and voltage at the MPP will always be equal to 1 p.u., resulting in a normalized (per unit) maximum power line (MPL) with a slope of $\tan\theta_M = I_M/V_M = 1$. If the p.u. value of the load current (array current) does not match the MPP current I_M, then the array operates at a different point from the MPP. For an operating current $I_C = I_{C2} > I_M$, the array operates in the overcurrent zone, resulting in lower output voltage V_{C2} with an operating power line (OPL) whose slope is greater than the slope of the MPL ($\theta_{C2} > \theta_M$). For an operating current $I_C = I_{C1} < I_M$, the angle θ_{C1} of the OPL becomes less than the angle θ_M of the MPL operating the array in the overvoltage zone, which means that the array current is too small for MPP operation. Neither the overcurrent nor the overvoltage operating zone is preferred as only the MPP operation is needed to get almost the maximum available power output from the PV array. Therefore, use of the error signal θ_e as an input to the controller is suggested. θ_e is defined as the difference between the angles θ_C and θ_M of the OPL and MPL, respectively:

$$\theta_e = (\theta_M - \theta_C) \tag{11}$$

where θ_M is held constant at 45° for all temperature levels and θ_C varies as a function of the electrical load current, the temperature, and solar irradiation levels. The controller is designed to minimize this error signal θ_e and hence operate the array at the MPP.

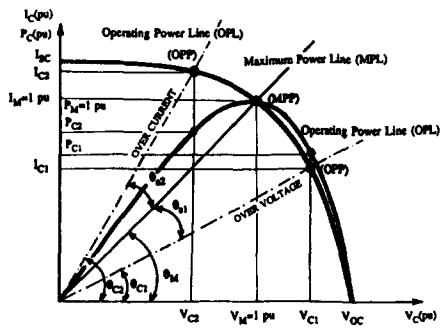

Fig. 4. $I-V$ and $P-V$ characteristics of a PV array including maximum power point and operating power point quantities.

3. The controllers

Both the PI and fuzzy logic controllers are utilized and assessed to calculate the chopper control signal V_{cont} which controls the duty cycle ratio α_D, hence compensates for the MPP error θ_e and ensures perfect tracking of available solar energy.

3.1. PI controller

The forward path of the PI controller is shown in Fig. 5. Depending on the control signal $U(k)$, the change in the chopper control signal, $dU(k)$, is obtained at each sampling period and is added to the previous control signal $V_{cont}(k-1)$ to find the new value $V_{cont}(k)$. When the array reaches the operating level θ_M or the MPP, the error signal θ_e becomes zero or very close to zero. Hence, the change in the chopper control voltage also becomes zero and the previous value of the control signal to the chopper remains unchanged. The controlled output of a PI controller is expressed as the sum of two signals related to the error:

$$U(t) = K_P\theta_e(t) + K_I\int \theta_e(t)\,dt \tag{12}$$

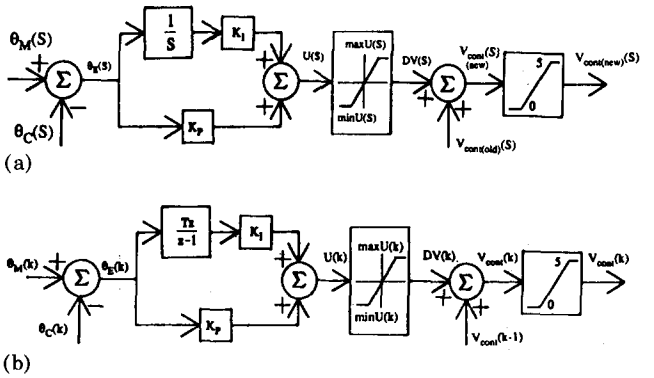

Fig. 5. Forward path of the PI controller: block diagram of the PI controller in (a) the S domain and (b) the z domain.

The first term in eqn. (12) is directly proportional to the error signal $\theta_e(t)$ with a gain of K_P. The second term is related to the integral of the same error signal with a gain of K_I. For a sampled system, the proportional part can be represented as follows:

$$U_1(k) = K_P\theta_e(k) \tag{13}$$

The integral part, however, must be solved numerically using numerical solution methods such as Euler's method, the trapezoidal method or Simpson's rule, etc. The use of Euler's method results in the following represention of the second part of eqn. (12) using the recursive formula:

$$U_2(k) = U_2(k-1) + K_I T\theta_e(k) \tag{14}$$

The total control signal obtained is

$$U(k) = U_1(k) + U_2(k) \tag{15}$$

where T and k are the discrete sampling period and the sampling counter number, respectively. The controller parameters $K_P = 0.05$ and $K_I = 0.05$ were selected such that the PM DC motor load starts smoothly without causing undesired inrush or overcurrent conditions. Owing to the integrator's presence in the controller, the control system may go into saturation unless the output signal of the PI controller is limited. Hence, the following lines must be added to the program:

IF $U(k) > U_{max}$ THEN

$U(k) = U_{max}$

$U_2(k) = U_{max} - U_1(k)$

IF $U(k) < U_{min}$ THEN

$U(k) = U_{min}$

$U_2(k) = U_{min} - U_1(k)$

$U_1(t)$ and $U_2(t)$ can be expressed in the z domain by

$$U_1(z) = K_P\theta_e(z) \tag{16}$$

$$U_2(z) = \frac{U_2(z)}{z} + K_I T\theta_e(z)$$

$$= \frac{z}{z-1} K_I T\theta_e(z) \tag{17}$$

The sampling delay is introduced by the term $z/(z-1)$ in the z domain. The total control output signal from the controller in the z domain is the sum of eqns. (16) and (17). The block diagrams representing the PI controller in the S and z domains are shown in Figs. 5(a) and (b), respectively.

3.2. *Fuzzy logic controller*

As shown in Fig. 6, the error signal $\theta_e(k)$ and its rate of change $d\theta_e(k)$ from the $(k-1)$th sample to the kth sample are the selected inputs to the fuzzy logic (FL) controller. First they are quantized into a common universe of discourse and their linguistic fuzzy subsets along with their membership grades are defined as shown in Fig. 7. This process is shown as the *fuzzifier* in Fig. 6. The FL control rules heuristically developed and given in Table 1 are implemented to yield the fuzzy subsets of the quantized output value $dU_Q(k)$ representing the change in the control input signal and their membership grades in

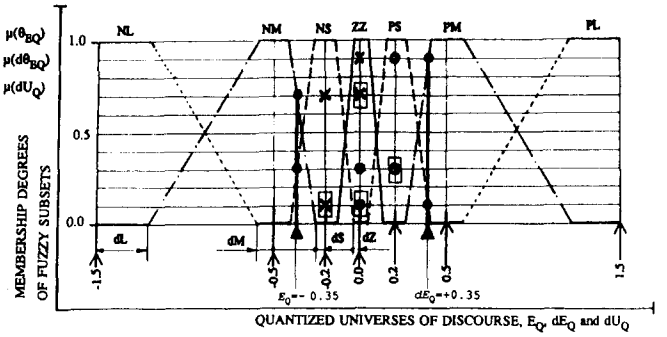

Fig. 7. Fuzzy subsets and their membership grades in the common universe of discourse.

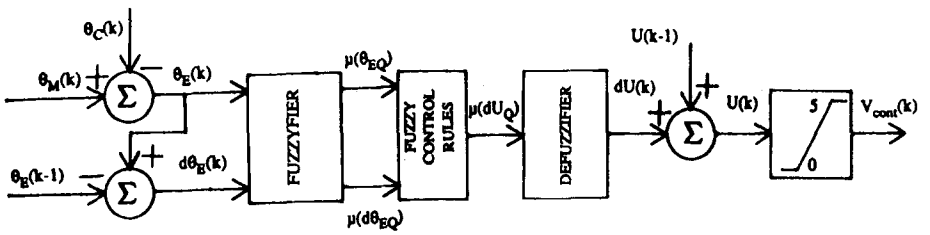

Fig. 6. Block diagram of the fuzzy logic controller.

TABLE 1. Fuzzy control rule decision table (the numbers are the fuzzy rule numbers)

	NL_{dE_Q}	NM_{dE_Q}	NS_{dE_Q}	ZZ_{dE_Q}	PS_{dE_Q}	PM_{dE_Q}	PL_{dE_Q}
NL_{E_Q}	NL_{dU_Q} 1	NL_{dU_Q} 2	NL_{dU_Q} 3	NM_{dU_Q} 4	NM_{dU_Q} 5	NS_{dU_Q} 6	ZZ_{dU_Q} 7
NM_{E_Q}	NL_{dU_Q} 8	NM_{dU_Q} 9	NM_{dU_Q} 10	NS_{dU_Q} 11	NS_{dU_Q} 12	ZZ_{dU_Q} 13	PS_{dU_Q} 14
NS_{E_Q}	NM_{dU_Q} 15	NM_{dU_Q} 16	NS_{dU_Q} 17	NS_{dU_Q} 18	ZZ_{dU_Q} 19	PS_{dU_Q} 20	PS_{dU_Q} 21
ZZ_{E_Q}	NM_{dU_Q} 22	NS_{dU_Q} 23	NS_{dU_Q} 24	ZZ_{dU_Q} 25	PS_{dU_Q} 26	PS_{dU_Q} 27	PM_{dU_Q} 28
PS_{E_Q}	NS_{dU_Q} 29	NS_{dU_Q} 30	ZZ_{dU_Q} 31	PS_{dU_Q} 32	PS_{dU_Q} 33	PM_{dU_Q} 34	PM_{dU_Q} 35
PM_{E_Q}	NS_{dU_Q} 36	ZZ_{dU_Q} 37	PS_{dU_Q} 38	PS_{dU_Q} 39	PM_{dU_Q} 40	PM_{dU_Q} 41	PL_{dU_Q} 42
PL_{E_Q}	ZZ_{dU_Q} 43	PS_{dU_Q} 44	PM_{dU_Q} 45	PM_{dU_Q} 46	PL_{dU_Q} 47	PL_{dU_Q} 48	PL_{dU_Q} 49

the same common normalized universe of discourse dU_Q. After defuzzification of these fuzzy subsets and their membership grades, the actual value $dU(k)$ of the control input change for the kth sample is obtained and added to the previous control input $U(k-1)$ to find the new control input signal $U(k)$. The final *defuzzification* is done using either the 'maximum of maxima' (MOM) principle or the 'center-of-area' (COA) method. The latter, center-of-area, method is applied by weighting the control action of each rule by the membership degree of the corresponding fuzzy subset as given by Bernard [14]. The fuzzy logic control rule decision table is organized so that the PM DC motor load starts smoothly as in the case of the PI controller. The operating control actions of the FL controller are explained below.

Fuzzy logic control action

Step 1. Specify and store the minimum and the maximum ranges of the error signal $E = \theta_e$, the error change $dE = d\theta_e$, and the control input change dU.

Step 2. If the minimum and maximum ranges of step 1 are different, then quantize them into a common universe of discourse using scaling factors such that the maximum and minimum limits of the quantized error signal E_Q, the quantized error change dE_Q, and the quantized control input change dU_Q are all the same, as shown in Fig. 7. In this example, the scaling factors were chosen as $SF_E = 1$ for the error signal E, $SF_{dE} = E_{max}/dE_{max} = 0.5$ for the error change dE, and $SF_{dU} = E_{max}/dU_{max} = 0.3$ for the control input change dU, where the maximum error $E_{max} = 1.5$ rad, the maximum error change $dE_{max} = 3$ rad, and the maximum control input change $dU_{max} = 5$ V.

Step 3. Define the symmetrical linguistic fuzzy subsets for E_Q, dE_Q, and dU_Q. Here, NL = negative large, NM = negative medium, NS = negative small, ZZ = zero, PS = positive small, PM = positive medium, and PL = positive large for the three quantized control variables E_Q, dE_Q, and dU_Q in the common universe of discourse as shown in Fig. 7.

Step 4. Calculate the error θ_e and error change $d\theta_e$ for the current sampling period and find their quantized values E_Q and dE_Q, respectively, in the common universe of discourse. For example, let $E_Q = -0.35$ and $dE_Q = +0.35$, as depicted in Fig. 7.

Step 5. Determine the corresponding fuzzy subsets $\{NL_{E_Q} \cdots PL_{E_Q}\}$ and $\{NL_{dE_Q} \cdots PL_{dE_Q}\}$ for E_Q and dE_Q, respectively. For the values given in step 4, the corresponding fuzzy subsets are NM_{E_Q} and NS_{E_Q} for the quantized error $E_Q = -0.35$ and PS_{dE_Q} and PM_{dE_Q} for the quantized error change $dE_Q = +0.35$.

Step 6. Determine the fuzzy membership degrees $\{\mu(NL_{E_Q}) \cdots \mu(PL_{E_Q})\}$ and $\{\mu(NL_{dE_Q}) \cdots \mu(PL_{dE_Q})\}$ for all of the fuzzy subsets of E_Q and dE_Q. For the example, $\mu(NM_{E_Q}) = 0.7$, $\mu(NS_{E_Q}) = 0.3$, $\mu(PS_{dE_Q}) = 0.1$, and $\mu(PM_{dE_Q}) = 0.9$. The membership degrees of all of the other fuzzy subsets are zero.

Step 7. Use the fuzzy control rule discrete decision table (Table 1) for each of the fuzzy subsets of the quantized error E_Q and the quantized error change dE_Q to find the relative fuzzy subsets and their membership grades for the quantized control input change dU_Q for all of the 49 rules. Also find the quantized values of the con-

trol input change dU_Q where the membership grades of the fuzzy subsets are unity. The rules are implemented on the basis of IF $\cdots$ THEN routines. For example, rule 12 is implemented as

IF (E_Q is NM) and IF (dE_Q is PS)

THEN (dU_Q is NS)

which can be written as

IF (NM_{E_Q}) and IF (PS_{dE_Q}) THEN (NS_{dU_Q})

The fuzzy membership grade of NS_{dU_Q} is obtained using Boolean algebra:

$$\mu(NS_{dU_Q}) = \min[\mu(NM_{E_Q}, \mu(NM_{dE_Q})]$$

From steps 5 and 6, it is clear that both the quantized error E_Q and the quantized error change dE_Q have two active fuzzy subsets having a non-zero membership degree. Hence, there are only four active fuzzy rules among the full 49 rules given in Table 1 for the example being used. Since the active fuzzy subsets of the quantized error are NM_{E_Q} and NS_{E_Q}, and the active fuzzy subsets of the quantized error change are PS_{dE_Q} and PM_{dE_Q}, only rules 12, 13, 19, and 20 will be active rules, resulting in four active fuzzy subsets, NS_{dU_Q}, ZZ_{dU_Q}, ZZ_{dU_Q}, and PS_{dU_Q}, of the quantized control input change. Thus,

from rules 1–11

$$\mu_{dU_Q}(i) = 0.0 \qquad i = 1, 2, \ldots, 11$$

from rule 12

$$\mu_{dU_Q}(12) = \min[\mu(NM_{E_Q}), \mu(PS_{dE_Q})] = 0.1$$

and $dU_Q(12) = -0.2$ for $\mu(NS_{dU_Q}) = 1$

from rule 13

$$\mu_{dU_Q}(13) = \min[\mu(NM_{E_Q}), \mu(PM_{dE_Q})] = 0.7$$

and $dU_Q(13) = 0.0$ for $\mu(ZZ_{dU_Q}) = 1$

from rules 14–18

$$\mu_{dU_Q}(i) = 0.0 \qquad i = 14, 15, \ldots, 18$$

from rule 19

$$\mu_{dU_Q}(19) = \min[\mu(NS_{E_Q}), \mu(PS_{dE_Q})] = 0.1$$

and $dU_Q(19) = 0.0$ for $\mu(ZZ_{dU_Q}) = 1$

from rule 20

$$\mu_{dU_Q}(20) = \min[\mu(NS_{E_Q}), \mu(PM_{dE_Q})] = 0.3$$

and $dU_Q(20) = 0.2$ for $\mu(PS_{dU_Q}) = 1$

from rules 21–49

$$\mu_{dU_Q}(i) = 0.0 \qquad i = 21, 22, \ldots, 49$$

As mentioned earlier, the control input change is determined using either the 'maximum of maxima' principle or the 'center-of-area' method. For the MOM method, the quantized value of the control input change is the one where the membership grade of the fuzzy subset with the highest membership grade in the universe of discourse is maximum, that is, unity in this case. From the above example, the fuzzy subset ZZ_{dU_Q} of rule 13 has the highest membership grade of $\mu_{dU_Q}(13) = 0.7$ among the other fuzzy subsets in the universe of discourse dU_Q. In equation form, from the above rules, the quantized control input change will be $dU_Q(n)$ for $\mu_{dU_Q}(n) = \max[\mu_{dU_Q}(i)]$, where $i = 1, 2, \ldots, 49$ and n is one of the i rules. For the worked example, $n = 13$ and $dU_Q(13) = 0.0$. Using the COA method, the quantized value of the control input change for the kth sample is determined as follows:

$$dU_Q(k) = \frac{\sum_{i=1}^{49} \mu_{dU_Q}(i)\, dU_Q(i)}{\sum_{i=1}^{49} \mu_{dU_Q}(i)} \tag{18}$$

For the above example over the entire rule base,

$$\begin{aligned} dU_Q(k) = {} & [0 + (0.1)(-0.2) + (0.7)(0.0) + 0 + (0.1)(0) \\ & + (0.3)(0.2) + 0]/(0 + 0.1 + 0.1 + 0 + 0.7 \\ & + 0.3 + 0) = 0.0333 \end{aligned} \tag{19}$$

Then, this quantized value $dU_q(k)$ is converted back to the actual level $dU(k)$ using the scaling factor that was used initially in the quantization process (step 2).

Step 8. Add the control input change $dU(k)$ to the previous value $U(k-1)$ to calculate the new control action to be taken for the kth sample:

$$U(k) = U(k-1) + dU(k) \tag{20}$$

Step 9. Keep the control input signal between 0 and 5 V as specified by the D/A board and the triggering control circuit of the MOSFET chopper.

4. The load

A permanent magnet (PM) DC motor driving a fan type load is used. The time domain equations

of the PM DC motor can be written as follows [15]:

$$\begin{bmatrix} \frac{di_a}{dt} \\ \frac{d\omega_m}{dt} \end{bmatrix} = \begin{bmatrix} -\frac{R_a}{L_a} & -\frac{K_v}{L_a} \\ \frac{K_v}{J_m} & -\frac{B_m}{J_m} \end{bmatrix} \begin{bmatrix} i_a \\ \omega_m \end{bmatrix} + \begin{bmatrix} \frac{V_a}{L_a} \\ -\frac{T_L}{J_m} \end{bmatrix} \tag{21}$$

where the nomenclature is as follows.

B_m damping coefficient (0.000432 N m s)
i_a motor current (no-load current = 1.62 A)
J_m inertia of rotor (0.000745 kg m^2)
K_v EMF constant (0.095) determined by strength of magnet, reluctance of iron and number of turns of armature winding
L_a armature inductance (0.00805 H)
R_a armature resistance (1.4 Ω)
T_L load torque, N m
V_a applied voltage to motor (rated voltage = 36 V)
ω_m motor speed (no-load speed = 356 rad/s)

The applied armature voltage to the motor is the controlled output voltage of the MOSFET chopper which has a chopping frequency of 20 kHz. The load torque to be used in the simulation is represented as a function of the motor speed by the general torque equation

$$T_L = K_1 + K_2\omega_m + K_3\omega_3^2$$

whose coefficients K_1, K_2, and K_3 are obtained by curve fitting the torque versus speed characteristics of the fan type load.

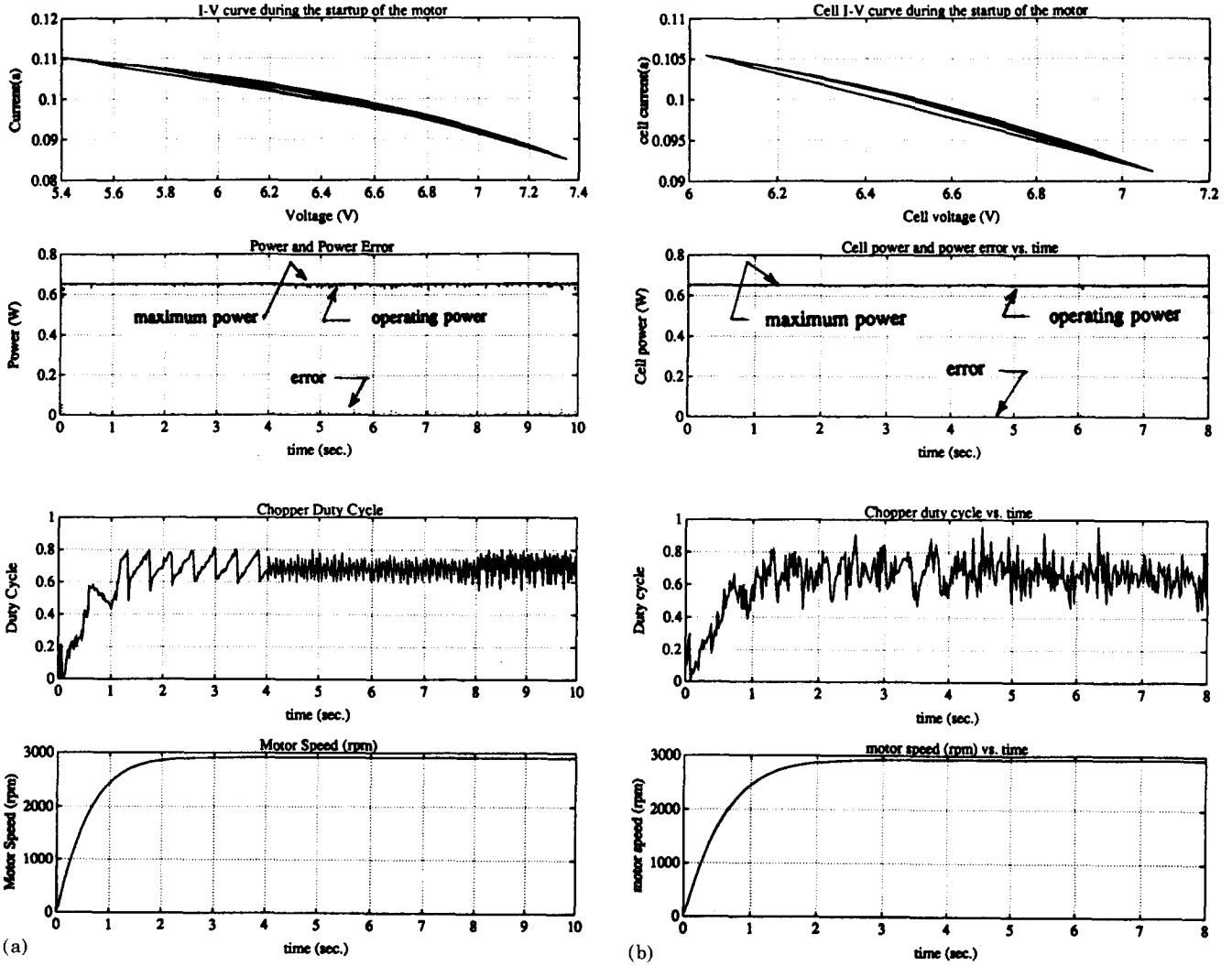

Fig. 8. Digital simulation results showing the responses of the solar cell $I-V$ curve, solar cell power, chopper duty cycle, and motor speed: (a) using the PI controller; (b) using the fuzzy logic controller.

5. Results

The digital simulation results and implementation oscillograms of the scheme shown in Fig. 1 are given in Figs. 8 and 9. The dynamic responses of the PV array $I-V$ characteristics, array power, chopper duty cycle α_D, and motor speed ω_m are presented for both the PI and the fuzzy logic controllers using the simulation and test results. The effects of the changing temperature on the $I-V$ curve and the solar irradiation levels on the PV array voltage, current, and power are also given for both the PI and FL controllers using the test data. It should be noted that the labels of the resultant Figures related to the PV array are not the actual values. These are the values of the reference array model data stored in the computer model. After D/A conversion, the array voltage is amplified by a gain of 15. Meanwhile, using a current transducer, the load current is converted to the reference analog voltage before the A/D conversion to the DT 2821 board. In order to have the same simulation and test models, this conversion process was included in the simulation model as well. As can be seen from Figs. 8(a) and (b), both controllers give almost identical simulation results. The MPP error has been minimized almost to zero so that the array operates at the MPP with very small fluctuations. The PI and FL controllers may be compared best using the duty cycle response since it is defined directly by the controllers. As

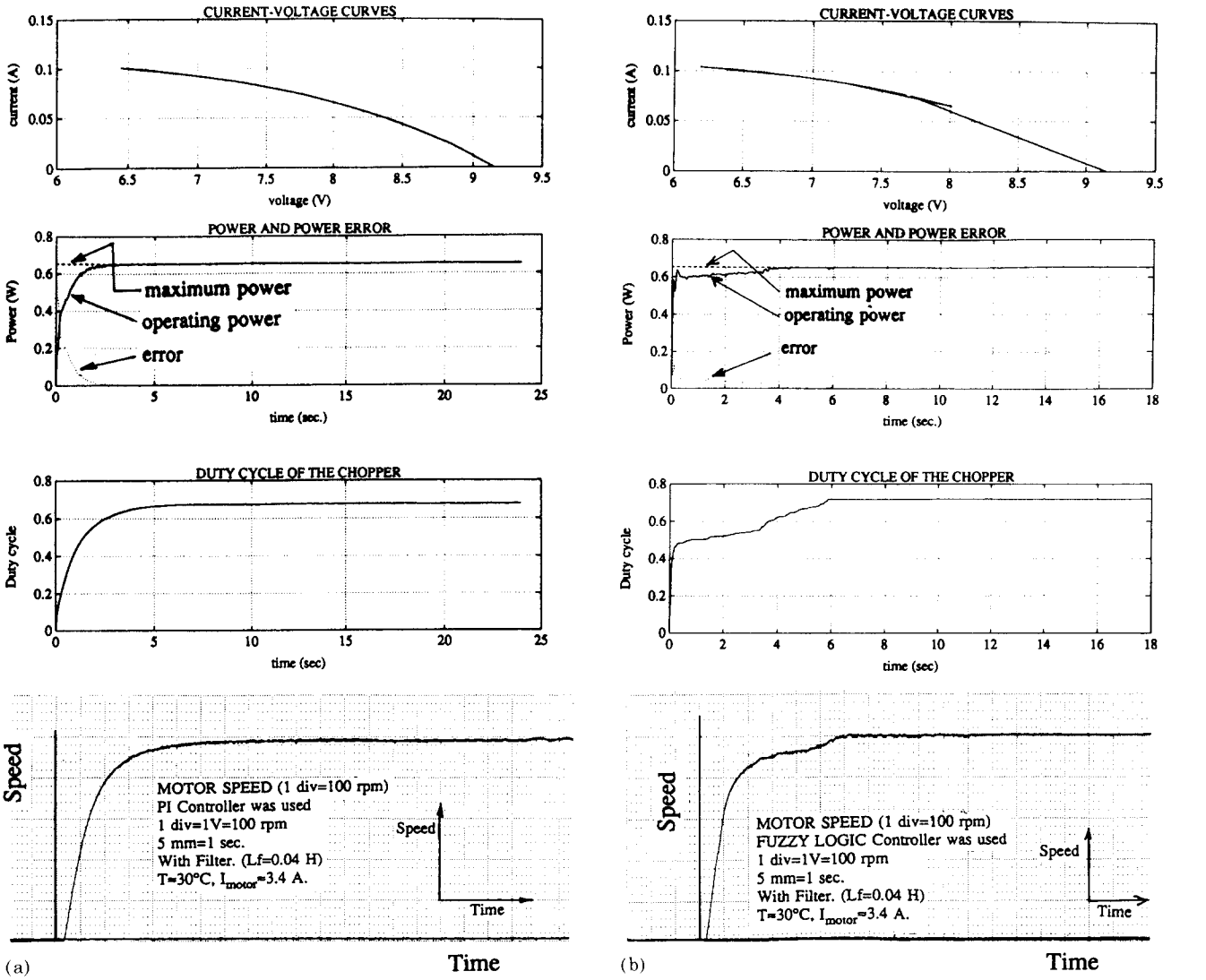

Fig. 9. Laboratory implementation results showing the responses of the solar cell $I-V$ curve, solar cell power, chopper duty cycle, and motor speed: (a) using the PI controller; (b) using the fuzzy logic controller.

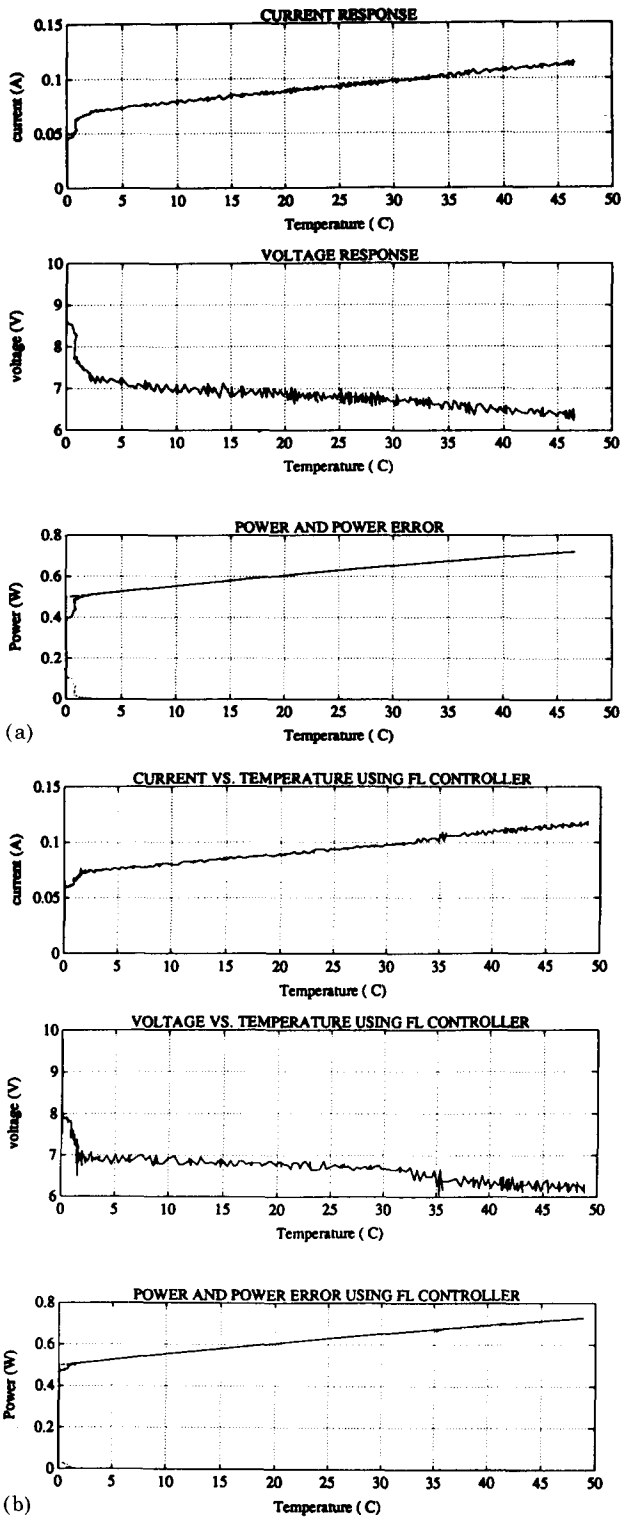

Fig. 10. Current, voltage and power responses of the solar cell as the temperature varies during the laboratory implementation: (a) using a PI controller; (b) using a fuzzy logic controller.

shown in Figs. 8 and 9, the duty cycle ratio α_D is increased slowly by both controllers until the array starts operating at the MPP. By increasing the duty cycle slowly, the applied voltage to the motor is increased step by step, so that the motor does not suffer any inrush overcurrent conditions and therefore any damage in the system is avoided. Duty cycle α_D fluctuations which appear in the simulation results do not appear in the experimental results. This is because of the additional filtering due to mechanical motor friction and the filter capacitors used in the chopper circuit that were not considered in the simulation model of the system. The speed responses from the two controllers are almost the same in the simulation. In the laboratory testing, the jumps from one fuzzy rule to another slow down the motor for a moment before it reaches steady-state operation. However, this problem may be eliminated by choosing and applying more properly selected fuzzy subsets and rules, more subsets, and more rules. The MPP line tracking scheme was achieved perfectly using either the PI or the FL controller for varying temperature conditions, as shown in Fig. 10. Temperature axes that indicate variable temperature in Fig. 10 also include the varying solar irradiation, as explained in §2. The MPP error θ_e is kept almost zero while the array operating power is increased for increasing temperature and irradiation. Therefore, it can be concluded that the proposed controllers are tracking the maximum available solar power of the PV array.

6. Conclusion

A novel fuzzy logic controller for PV array maximum power tracking has been investigated and compared with the classical PI controller. The conversion scheme consisting of a PV array, a power amplifier, a DC chopper, and a PM DC motor driving a fan type load was digitally simulated and laboratory tested. It has been shown that the PV array can be operated at its maximum available reference solar power point under any temperature or solar irradiation level changes. This goal is achieved by controlling the array output voltage to the PM DC motor load using the chopper converter so that the load current always matches the array maximum power operating reference current. The load voltage is controlled using a DC chopper between the PV array and the load. This chopper acts as a special variable ratio voltage/voltage transformer. Satisfactory results were obtained using either classical PI or fuzzy logic controllers to control the DC chopper. The novel fuzzy logic

design can be extended to other power system applications such as voltage control, power system stabilizers, and coordinated speed control applications.

References

1 M. Buresch, *Photovoltaic Energy Systems Design and Installation*, McGraw-Hill, New York, 1983.

2 Z. M. Salameh and F. Dagher, The effect of electrical array reconfiguration on the performance of a PV powered volumetric water pump, *IEEE Trans., EC-5* (1990) 653–658.

3 J. A. Roger, Theory of the direct coupling between DC motors and photovoltaic solar arrays, *Solar Energy, 23* (1979) 193–198.

4 W. Z. Fam and M. K. Balachander, Dynamic performance of a DC shunt motor connected to a photovoltaic array, *IEEE Trans., EC-3* (1988) 613–617.

5 J. Appelbaum, Starting and steady-state characteristics of DC motors powered by solar cell generators, *IEEE Trans., EC-1* (1986) 17–25.

6 I. H. Altas and A. M. Sharaf, A solar powered permanent magnet DC motor drive scheme, *Proc. 17th Annu. Conf. Solar Energy Soc. Canada, Toronto, Ont., Canada, 1991*, pp. 65–70.

7 A. M. Sharaf and L. Wang, A photovoltaic powered efficient DC motor drive for pump irrigation, *Proc. Canad. Solar Energy Conf., Halifax, N.S., Canada, 1990.*

8 E. H. Mamdani and S. Assilian, An experiment in linguistic synthesis with a fuzzy logic controller, *Int. J. Man–Mach. Stud., 7* (1975) 1–13.

9 E. H. Mamdani, Application of fuzzy algorithms for control of simple dynamic plant, *Proc. Inst. Electr. Eng., 121* (1974) 1585–1588.

10 E. H. Mamdani, Advances in the linguistic synthesis of fuzzy controllers, *Int. J. Man–Mach. Stud., 8* (1976) 669–678.

11 L. A. Zadeh, Fuzzy sets, *Information Control, 8* (1965) 338–353.

12. L. A. Zadeh, Outline of a new approach to the analysis of complex systems and decision processes, *IEEE Trans., SMC-3* (1973) 28–44.

13 J. Maiers and Y. S. Sherif, Applications of fuzzy set theory, *IEEE Trans., SMC-15* (1985) 175–189.

14 J. A. Bernard, Use of rule based system for process control, *IEEE Control Syst. Mag.*, (Oct.) (1988) 3–13.

15 P. C. Krause and O. Wasynczuk, *Electromechanical Motion Devices*, McGraw-Hill, New York, 1989.